Electronic Supplementary Information for:

Intermolecular States in Organic Dye Dispersions: Excimers vs Aggregates

A. J. Musser[a]*, S. K. Rajendran[b], K. Georgiou[a], L. Gai[c], R. T. Grant[a], Z. Shen[c], M. Cavazzini[d], A. Ruseckas[b], G. A. Turnbull[b], I. D. W. Samuel[b], J. Clark[a] and D. G. Lidzey[a]

[a] Department of Physics and Astronomy, The University of Sheffield, Sheffield, United Kingdom

[b] Organic Semiconductor Centre, SUPA, School of Physics and Astronomy, University of St. Andrews, St. Andrews, United Kingdom

[c] State Key Laboratory of Coordination Chemistry, Collaborative Innovation Center of Advanced Microstructures, Nanjing University, Nanjing 210093, China

[d] Instituto di Scienze e Tecnologie Molecolari (ISTM), Consiglio Nazionale delle Ricerche (CNR), via C. Golgi 19, 20133 Milan, Italy

Email: a.musser@sheffield.ac.uk

Contents

1. Synthesis of BODIPY dyes E1-3, A1-3

BODIPY dyes E1,[1] E2,[2] E3,[3,4] A1,[5,6] A2[7] and A3[8] were synthesized as per previous reports.

2. Steady-State Characterization

2.1 UV-Vis Absorption

Absorption spectra were measured for all films reported in main-text Fig. 1. The primary effect of increased concentration is broadening of the main BODIPY absorption band ~2.5 eV, which is partially responsible for the apparent rise of the 0-1 vibronic peak. Absorption in this region has also been attributed to dark H-aggregates. There is no evidence in UV-Vis absorption for the low-energy emissive states discussed in the main text; these are present in such small population that only more sensitive PL-based measurements can detect them.

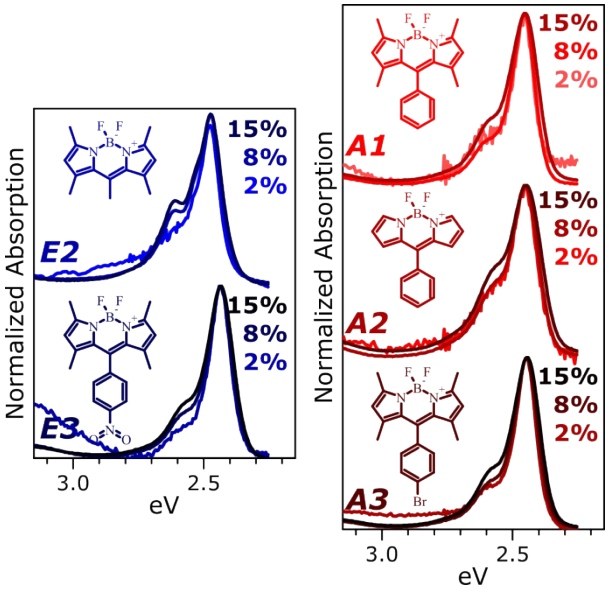

Figure S1. Concentration-dependent UV-Vis absorption of BODIPY films. Increasing concentration primarily results in slight broadening of the absorption bands, resulting in an increase in the 0-1 spectral peak. Variation at high energies, particularly in low-concentration films, reflects uncertainty in the background subtraction because of the extremely small absorption signal. Equivalent results for E1 have been previously reported.[9]

2.2 PL Quantum Efficiency

The concentration-dependent PL quantum efficiency was measured for BODIPY derivatives A1-3 and E2-3 using an integrating sphere coupled to an Oriel MS-125 1/8m spectrograph. Concentration quenching was observed to varying degrees in all materials, which we largely attribute to the non-radiative decay pathways present in the excimer state. The 'saturation' efficiency in all films is high, due to the contribution of emissive sub-gap states.

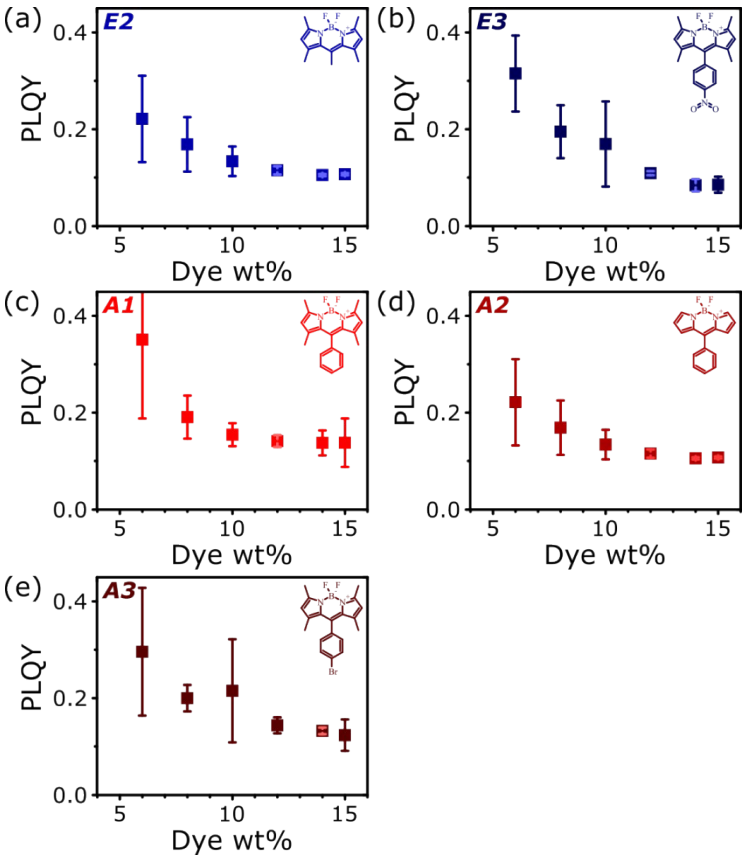

Figure S2. PL Quantum Yield of BODIPY films. Integrated steady-state PL efficiency measured as a function of concentration of (a) E2, (b) E3, (c) A1, (d) A2 and (e) A3 in polystyrene matrix. Error bars reflect variability of results with film thickness (200 and 300 nm). Equivalent results for E1 have been previously reported.[9]

2.3 Identification of Intermolecular Components

The PL spectrum of species arising from intermolecular interactions was determined by comparison of concentrated and dilute films of E1 and A1. To ensure robustness of the comparison, it was performed separately for seven temperatures over the range 100-295 K. Briefly, the temperature dependence of PL in high- and low-concentration films (Fig. S3a-d) was measured for each molecule. In high-concentration films, the distinctive red-shifted emission of excimers and aggregates was accompanied by a pronounced growth in PL intensity and slight blue-shift upon cooling (from coloured to black). By contrast, in dilute monomer-only films we observed a relatively modest increase in PL intensity and slight red-shift (from coloured to grey). There was no substantial change in the UV-Vis absorption spectrum over this temperature range (Fig. S3e-f). To isolate the intermolecular component, we scaled the dilute-film monomer emission point-by-point by the high-concentration film transmission, as an approximate correction for the expected contribution of self-

absorption. The resulting spectrum was then scaled to give the best fit to the high-concentration spectrum. As shown in Fig. S4, the resulting match is strong, and the self-absorption correction very closely accounts for the shift in PL spectral edge at high concentrations. The residual emission in the high-concentration films is assigned to the intermolecular components; the spectra presented in main-text Fig. 2c and Fig. S5 are the result of subtraction of the spectra in Fig. S4.

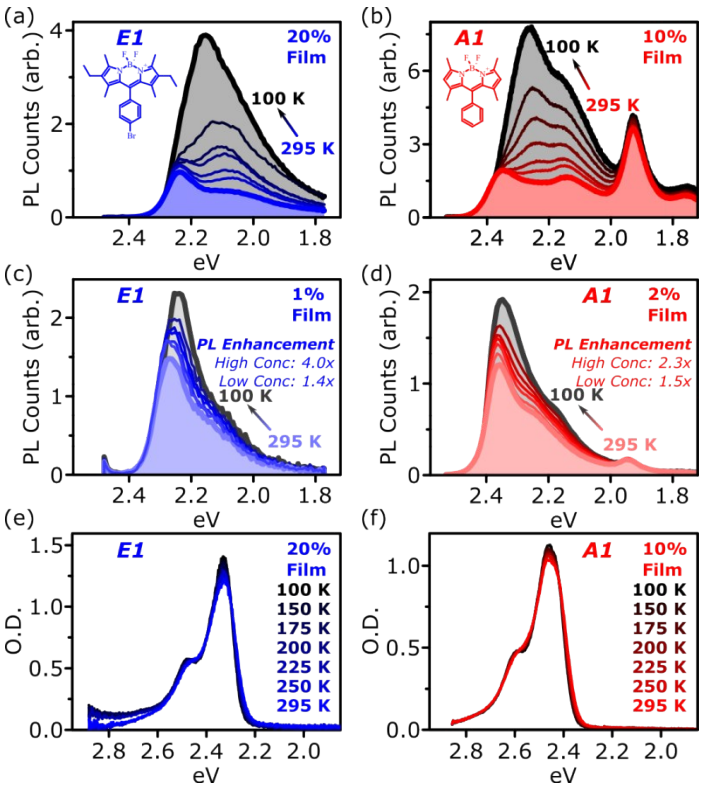

Figure S3. Temperature-dependent PL spectra of high-concentration films of (a) E1 and (b) A1 reproduced from main-text Figure 2. Dilute films of (c) E1 and (d) A1 show much smaller spectral shifts and negligible changes in shape (slight narrowing). The PL efficiency is increased ~1.5x upon cooling to 100 K in the dilute films, and 2-4x in the concentrated films, all of which suggest the changes observed in high-concentration films arise from intermolecular interactions. Temperature-dependent absorption in high-concentration (e) E1 and (f) A1 films shows no such variation; the temperature-dependent effects observed in PL are purely excited-state phenomena.

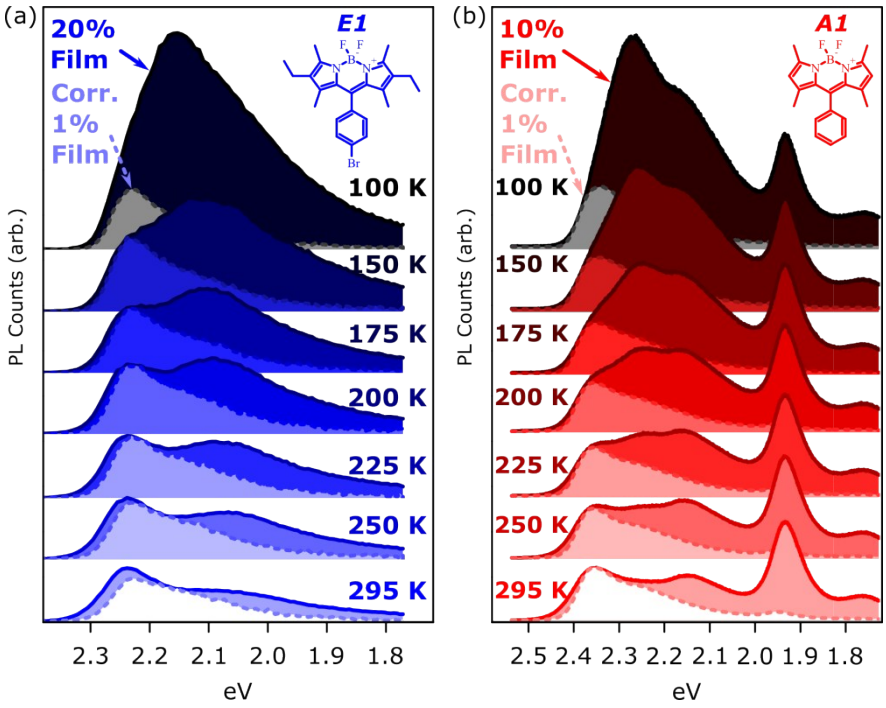

Figure S4. Comparison of raw PL from high-concentration films (dark) with scaled and corrected PL from low-concentration films (light) shows good agreement with the high-energy edge of the emission in (a) E1 and (b) A1 films, given the simplicity of the spectral correction. The low-concentration film PL was multiplied by the temperature-dependent % transmission at each wavelength (Fig S1e,f). This component is attributed to non-interacting molecules in the high-concentration films and is assigned as the monomer component in each. We note that the monomer contribution to the spectrum remains ~constant throughout the temperature range, suggesting the process of monomer quenching (forming excimers or aggregates) is largely temperature-independent. This is in accord with the ~invariant kinetics of monomer decay upon cooling discussed in the main text. The increase in PL efficiency at lower temperature reflects this shifting balance of radiative and non-radiative decay channels in the red-shifted excimer states.

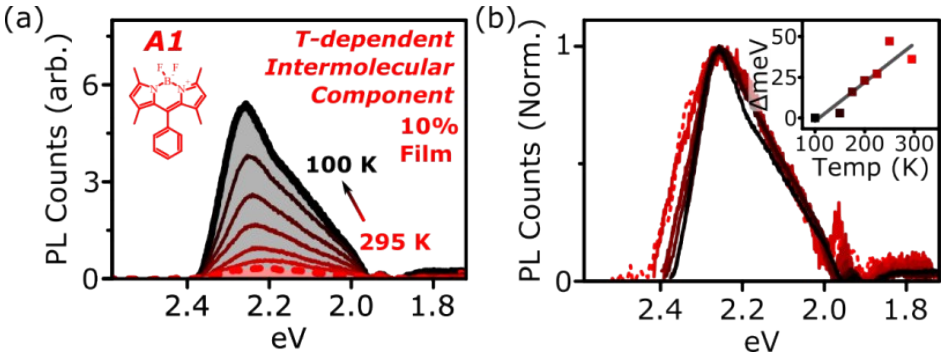

Figure S5. Isolation of A1 excimer component. (a) The temperature-dependent component of the data in main-text Fig. 2d was estimated by subtracting the 295K spectrum from those at other temperatures, scaled at each temperature to minimize the residual ~1.95 eV. The small residual is due to slight variation of the peak upon cooling. We justify the use of the 295 K spectrum to represent the temperature-independent component based on the close match of that spectrum to the 'SGE' species extracted from streak-camera measurements, as shown in main-text Fig. 7. Dashed spectrum is the excimer extracted from streak-camera measurements, for comparison. (b) Temperature-dependent intermolecular (i.e. excimer) spectra, normalized and blue-shifted to overlap with the spectrum at 100 K. The degree of shift is approximately linear with temperature, as in E1, though the overall shifts are smaller. The similarity of spectral shape over the temperature range and to the excimer in E1 suggests a common electronic origin.

2.4 PL Excitation Mapping

PL excitation measurements were performed for low- and high-concentration films of E1 and A1 over the full temperature range, scanning excitation wavelength from 390 nm to 600 nm (E1) or 650 nm (A1) and detection wavelength from ~500 nm to 700 nm (E1) or 750 nm (A1). No significant temperature dependence was identified beyond that already evident from the single-excitation spectra above and in the main text, so we only present representative data from 200 K here. No signatures of any sub-gap absorbing state could be identified in E1, confirming that the red-shifted emissive species must be an excimer (i.e. a dimer only in the excited state). The same is true for the intermediate emitter in concentrated A1 films, but we do detect a weak PL excitation signal corresponding to sub-gap excitation at 550-600 nm and emission at ~640 nm, i.e. the aggregate dimer peak. There is thus a weak ground-state absorption associated with this most red-shifted PL band, confirming its identity as aggregate rather than excimer. This feature was studied in more detail on a more sensitive instrument, as presented in main-text Fig. 2f. The data in Figs. 2f and S8 reveal that the sub-gap emitter is in fact two distinct electronic species. There are two well-defined vibronic peaks at low energy which can be described as a J-aggregated dimer, and the LEMS emission at 2.0-2.2 eV can be selectively enhanced with excitation near the presumed LEMS absorption (i.e. slightly higher energies than the detected emission).

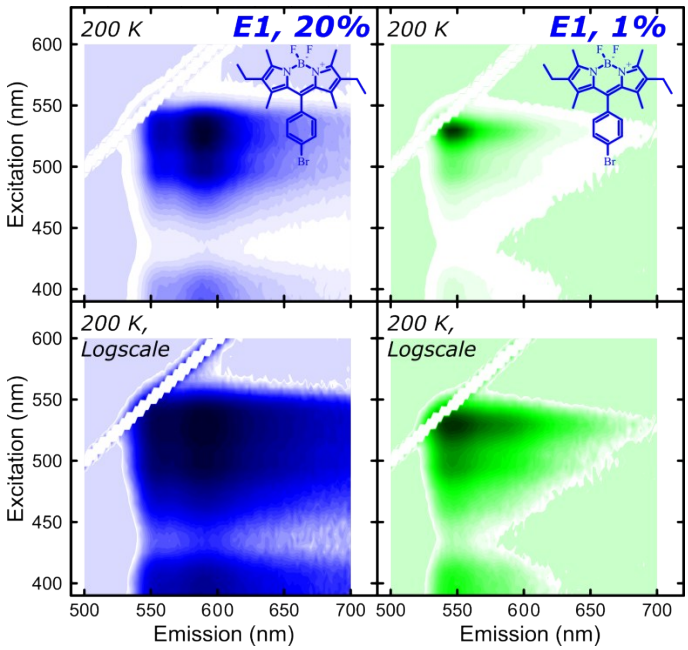

Figure S6. PL excitation maps of concentrated (left, blue) and dilute (right, green) E1 films, at 200 K, with linear (top) or logarithmic (bottom) intensity scale. At 200 K the separate excimer emission can be clearly distinguished (< 580 nm), but it has not yet blue-shifted as to overlap with the monomer emission. The apparent excitation band-gap is the same, and even in logscale no 'sub-gap' absorption corresponding to the red-shifted species can be detected. The low-energy emission is generated through excitation of the same monomer absorption spectrum, and it is thus assigned as an excimer state. The same is true across the full temperature range studied here (see Grant et al., Adv. Opt. Mater. 2016).

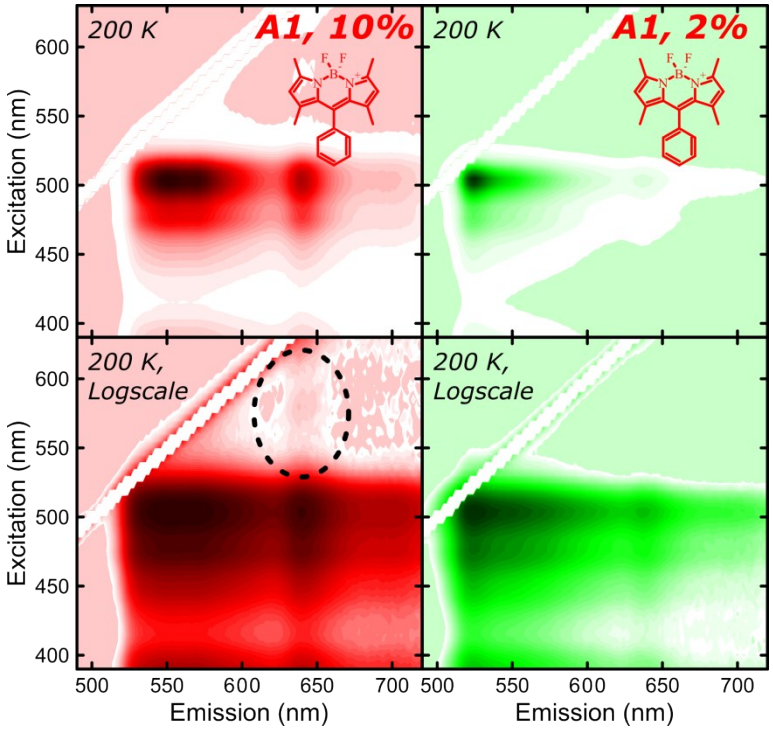

Figure S7. PL excitation maps of concentrated (left, red) and dilute (right, green) A1 films, at 200 K, with linear (top) or logarithmic (bottom) intensity scale. The 2% film is not sufficiently dilute to eliminate all signatures of dimer emission near 640 nm, but the strong enhancement of aggregate-related features in the concentrated film makes this a valid comparison nonetheless. The apparent excitation band-gap is the same for most of the spectrum, enabling assignment of the strongly temperature-dependent species peaked ~550 nm to excimers, as in E1 above. However, in the concentrated film an additional weak excitation feature is found (dashed), corresponding to excitation 550-600 nm and emission from the peak at ~640 nm. This red-shifted feature, which exhibits clear vibronic structure and can be directly excited from the ground state, is assigned to aggregated dimers. We note that the PL excitation spectra for monomer, excimer and SGE emission regions (i.e. ~530 nm, ~580 nm and ~640 nm) are almost identical in shape apart from the sub-gap feature indicated, even though the emission is dominated by the intermolecular species. This is a sign of efficient energy transfer through the film.

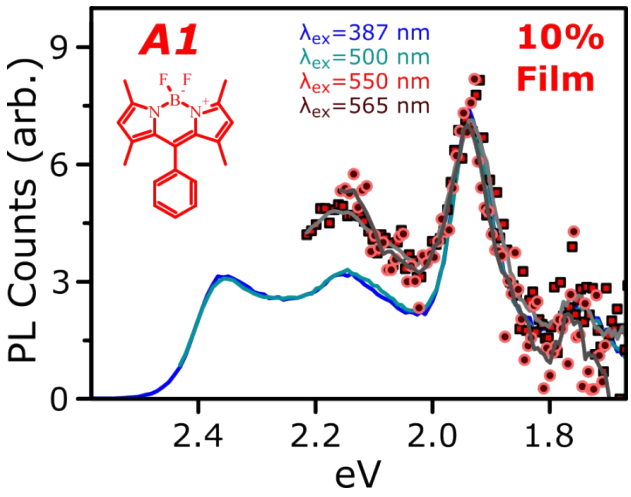

Figure S8. Sub-gap excitation in concentrated A1. PL spectra of 10% A1 film at room temperature, at a range of excitation wavelengths, measured on a more sensitive instrument than in Figures S6-7. Spectral shape does not change for excitation at 500 nm vs 387 nm. Sub-gap excitation at 550 nm and 565 nm yields the same dominant dimer peak at 1.95 eV, but also distinct enhancement in the LEMS emissive band 2.0-2.2 eV. This confirms that this higher-energy component to the 'SGE' spectrum is a distinct species from the J-type dimer bands that also exists in the ground state, in agreement with the model in main-text Fig. 7.

3. Time-Resolved PL

Streak camera measurements were performed on concentrated films of all derivatives. We also measured the concentration dependence for films of E1 and A1, and a full temperature dependence (100-295 K) of concentrated films of E1 and A1. There were no signs of variation in low-temperature measurements of dilute E1 films, so those results receive no further consideration. From the steady-state results and dynamics detected at room temperature in all E-class and A-class films, we consider E1 and A1 to be good models for their respective classes. Dynamics on longer timescales were studied using a time-correlated single-photon counting (TCSPC) system from Edinburgh Instruments.

3.1 Spectral Decomposition

We used singular value decomposition (Fig. S9) to determine the number of spectrally distinct species, and the datasets in main-text Fig. 3 fell into two groups: E-class films exhibited two well-defined species above the noise floor, while A-class films had three such species. The same procedure was used to analyse temperature-dependent data, with equivalent results. To further ensure the robustness of the spectral decomposition, we used the extracted spectra and kinetics to reconstruct the full 2D map. We find a close match to the raw data throughout the decay range (compare dashed and solid in Fig. S10), with very small residuals. We could not achieve this close match with a reduced number of species.

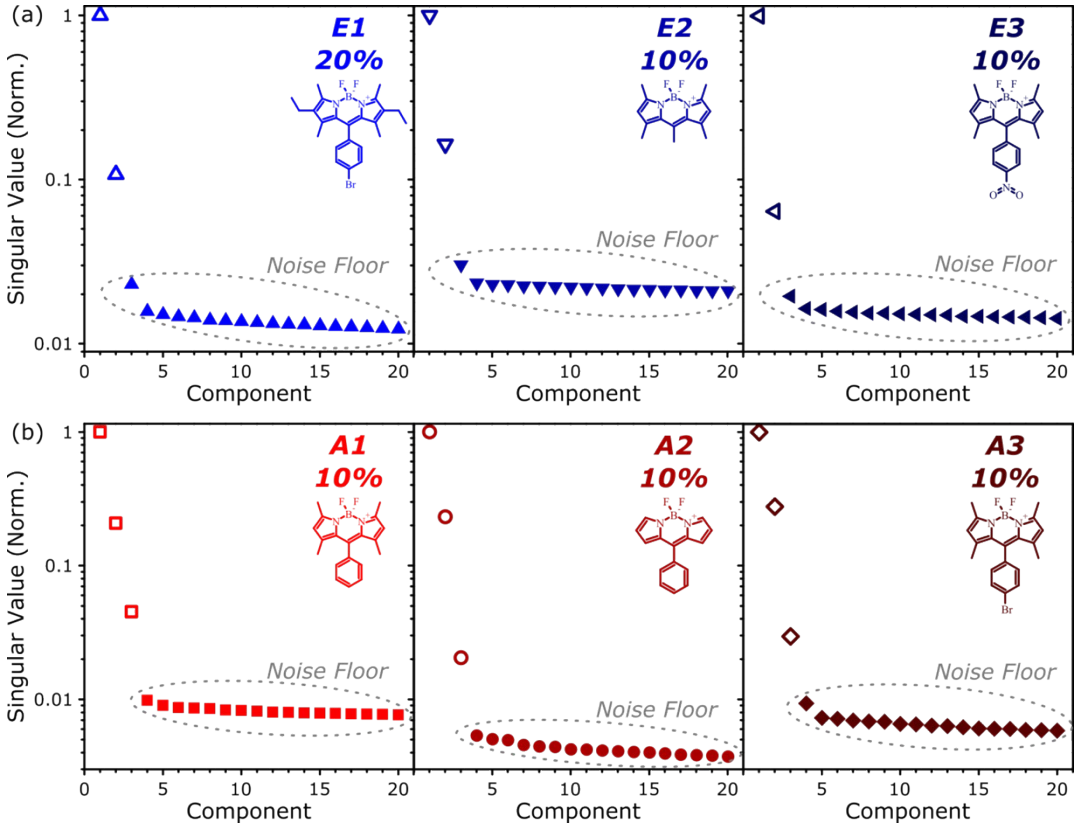

Figure S9. Determination of the number of spectrally independent species. Singular value decomposition was performed on every time-resolved PL map to reveal the number of principal components, i.e. spectral species, with their relative contribution to the data weighted by the singular value shown. (a) In concentrated E-class films, two strong species (open symbols) could be distinguished above the components corresponding to noise (solid). Results for E1 are equivalent over the full temperature series. (b) In concentrated A-class films, there were three such components. In all films the strongest component within the noise floor was also investigated, but this was found to contain no significant spectral features. The same results were found for A1 across the full temperature range.

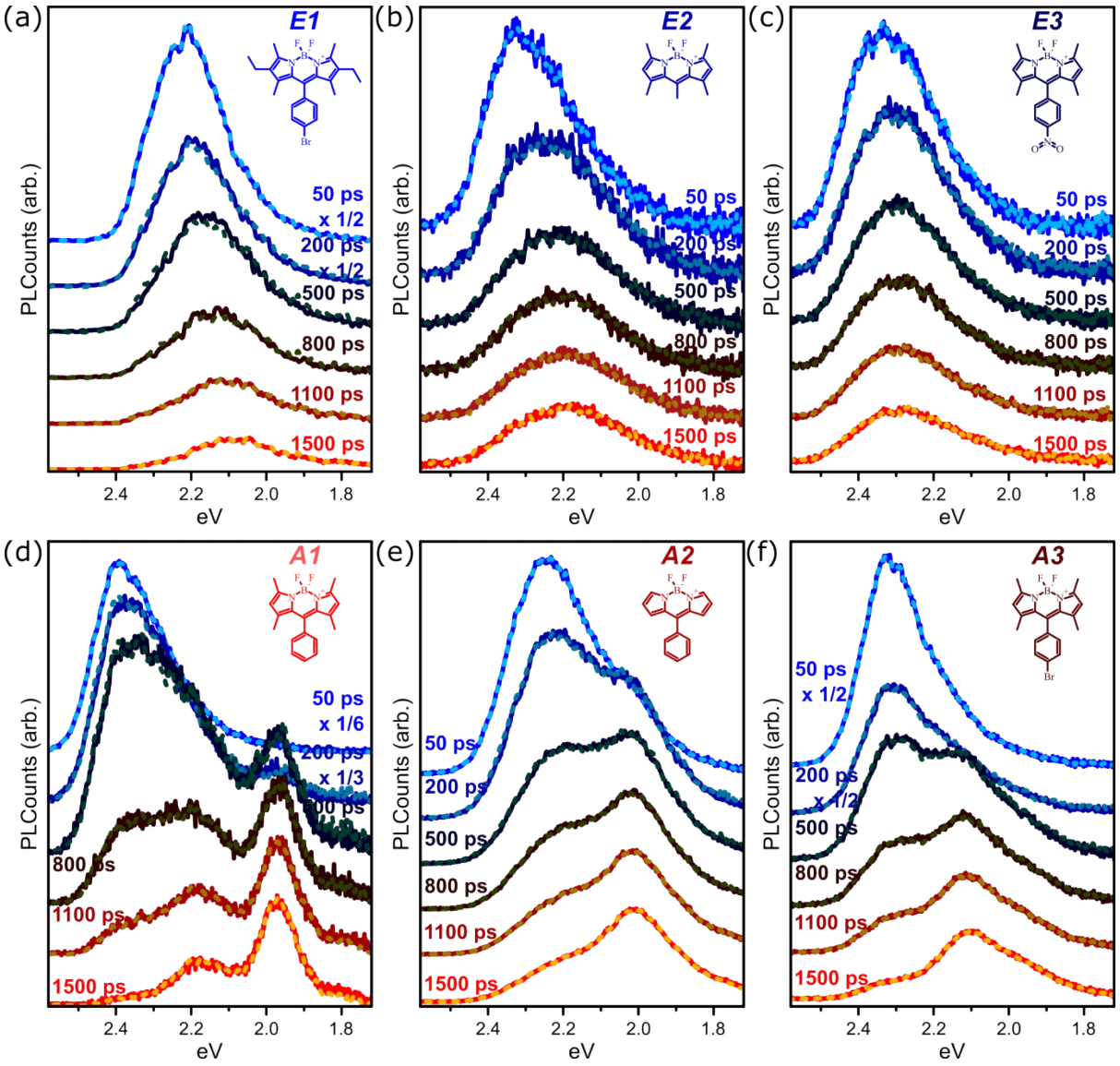

Figure S10. Comparison of raw time-resolved PL data (solid) and a reconstruction from the spectral decomposition illustrated in main-text Fig. 6 (dashed). The two-species model for (a) E1, (b) E2 and (c) E3 affords a close fit to the data on all timescales. Likewise, the three-species model for (d) A1, (e) A2 and (f) A3 closely follows the full spectral evolution. Spectral cuts are taken from the data in main-text Fig. 3. All measurements were performed on 10% films at 295 K, except E1 which was a 20% film at 200 K. For clarity, some spectra are scaled by a factor of 1/6-1/2 as indicated.

3.2 Concentration Dependence

We measured E1 films ranging from extremely dilute (0.1%) to very concentrated (20%). As expected, increasing the concentration progressively speeds the monomer PL decay. However, because of the low PL efficiency of the excimer state at room temperature, it is only from 10% loading that we are able to distinguish distinct excimer emission. The contribution at 5% may be apparent in a slight broadening and shift on long timescales, but the changes are too small for a clear determination. These effects are summarized in main-text Fig. 4.

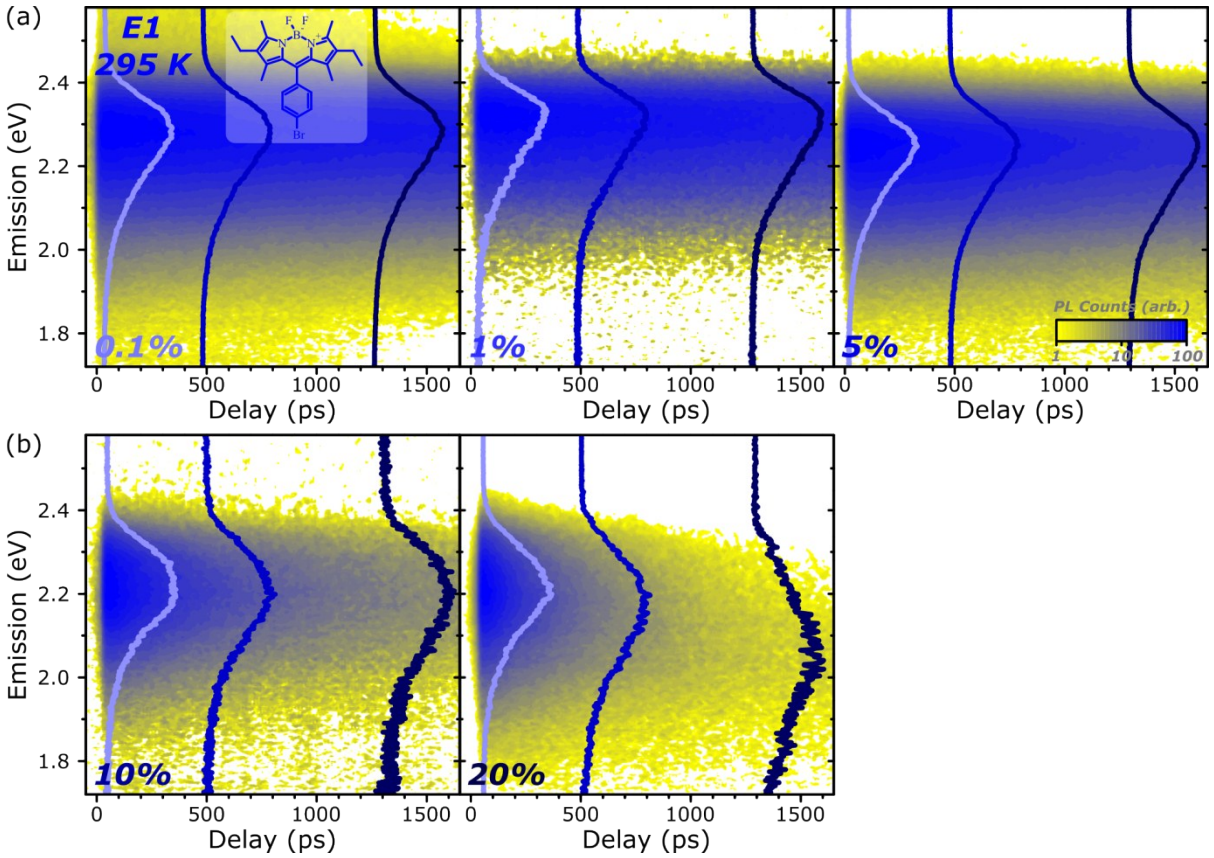

Figure S11. Concentration dependence of PL dynamics in E1 films. (a) Full streak-camera measurements in the dilute regime. Only monomer emission can be detected, though very slight changes in spectral shape can be observed at 5% on long timescales. (b) Full streak-camera measurements in the concentrated regime. There is a distinct red-shift and broadening on long timescales, due to efficient excimer formation. Normalised spectral cuts (lines; light blue: 50 ps, blue: 200 ps, dark blue: 1500 ps) highlight the evolution of emissive species. Selected cuts and PL decay kinetics extracted from these maps for main-text Fig. 4. Colour maps are presented with logarithmic intensity scale to highlight contribution from weak, long-lived species.

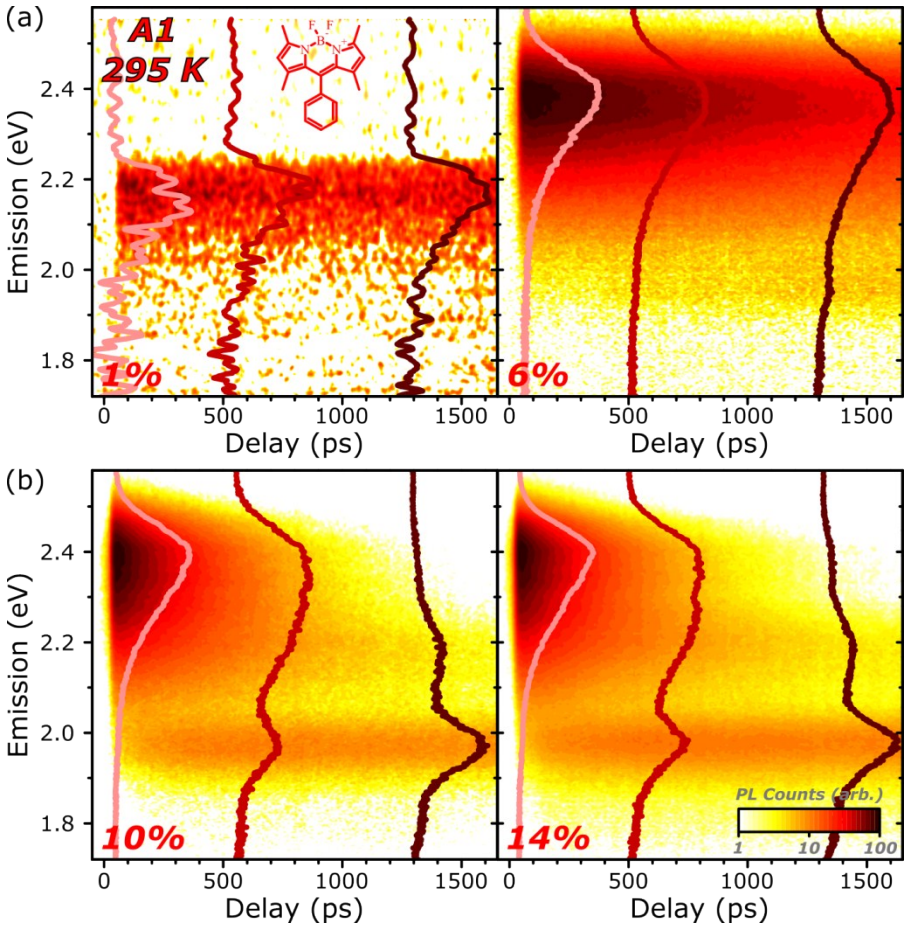

Figure S12. Concentration dependence of PL dynamics in A1 films. (a) Full streak-camera measurements in the dilute regime. 1% film was measured in photon counting mode with an additional colour filter blocking light >2.25 eV. It is nonetheless clear that only monomer emission is present, with no significant decay or spectral evolution over the timescale. Very slight changes in spectral shape can be observed at 6% on long timescales, suggesting slow aggregate formation. (b) Full streak-camera measurements in the concentrated regime. Initial monomer is rapidly converted into both excimer and aggregate states. This process is slightly faster in 14% films. Normalised spectral cuts (lines; light blue: 50 ps, blue: 200 ps, dark blue: 1500 ps) highlight the evolution of emissive species. Colour maps are presented with logarithmic intensity scale to highlight contribution from weak, long-lived species.

3.3 PL Anisotropy Dynamics

In order to probe the role of exciton migration, we studied the PL anisotropy decay dynamics in films of E1 and A1. In these experiments, we placed a polariser after the sample and optimised this for detection on the streak camera. We then performed measurements with the pump polarised either parallel or perpendicular to this polarisation, which in our isotropic films is equivalent to scanning the detection polarisation for a particular pump polarisation. From these measurements we determine the transient PL anisotropy using:

$$\gamma = \frac{PL_{\parallel} - PL_{\perp}}{PL_{\parallel} + 2 * PL_{\perp}}$$

In our system, in the absence of any exciton diffusion or conversion into emissive states with different transition dipole moment, we can expect a maximum value of 0.4. Any reduction from this value is a sign of migration of the excited state through the film, where it will sample sites with transition dipole completely uncorrelated from the initially sampled population, or of formation of new excited states with a differently orientated transition dipole moment. In very dilute films of E1 (0.1%, Fig. S13a), we observe a relatively large, long-lived PL anisotropy consistent with largely isolated molecules. An increase of the concentration to 1% (Fig. S13b) does not significantly affect the population decay kinetics (main-text Fig. 4) but clearly activates substantial exciton migration: the PL anisotropy is already very small beyond the instrument response timescale and rapidly decays to zero. This is consistent with the large oscillator strength and small Stokes shift of BODIPY dyes, which enables rapid, long-distance exciton migration through the film. Interestingly, at still higher concentrations we do observe some long-lived polarisation memory (Fig. S13c). This suggests that some excitons do not diffuse far before reaching a site capable of forming excimers (at which point they are trapped), and thus do not achieve fully randomised polarisation. However, it is significant to note that the primary PL anisotropy decay (from an initial value of 0.4) is markedly faster than the timescale for excimer formation. It is likely that the bulk of the excimer population is formed only after quite long-distance exciton migration. A similar picture emerges in concentrated films of A1 (Fig. S13d). Again the decay of PL anisotropy (from the initial value of 0.4) is much faster than the formation timescales of excimer and aggregate species, though in this case there appears to be no long-lived polarisation memory. We speculate that the density of long-lived emissive sites in these films is sufficiently low that virtually all excitations must undergo substantial migration before reaching them.

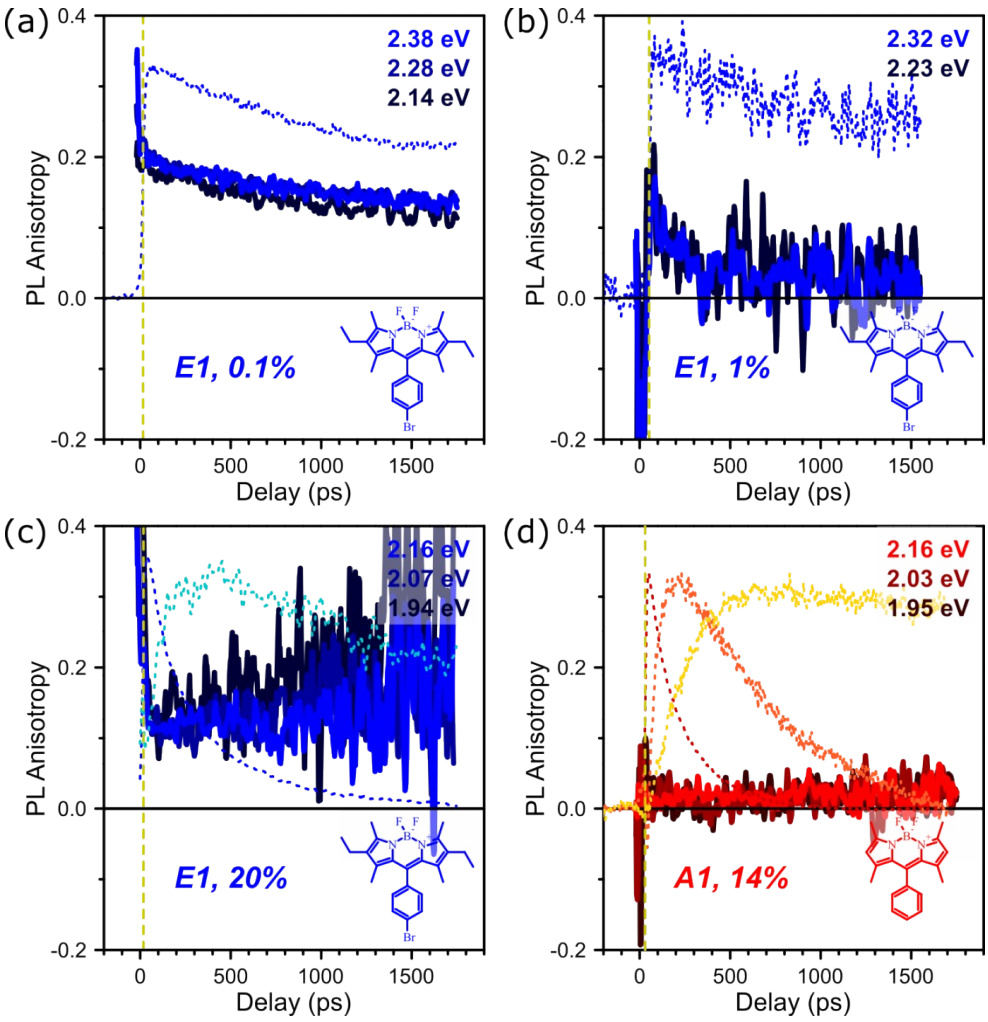

Figure S13. Polarisation memory in BODIPY films. The PL anisotropy was measured for E1 films at (a) 0.1%, (b) 1% and (c) 20% loading and provides direct evidence of rapid exciton migration. Likewise, the rapid loss of polarisation memory in (d) A1 films at 14% loading reveals that exciton migration occurs faster than the population conversion into excimers and/or aggregates. Dashed kinetics in panels (a) and (b) are raw PL decays (arb. scale) showing monomer emission dynamics. In panels (c) and (d) these are extracted monomer, excimer and aggregate population kinetics. Vertical dashed lines indicate the midpoint of the instrument response; in all films >50% of the polarisation memory is lost within the instrument response.

3.4 Temperature Dependence

The fast PL dynamics of both E1 (20%) and A1 (10%) films were studied over the temperature range 100-295 K. As described in the main text, E1 exhibited a progressive increase in the excimer band intensity as the film was cooled, but no major change in the monomer-to –excimer conversion time constant. This observation is consistent with the increasing excimer contribution to the steady-state PL arising from a reduction in the non-radiative decay rate, while the mechanism of excimer formation itself is little affected. We observe a slight blue-shift of the excimer emission band (observed on long timescales, 1500 ps in Fig. S14) concomitant with its increase in intensity. In A1 (Fig. S15) we observe qualitatively similar effects: the excimer band grows in relative intensity upon cooling, while its formation kinetics remain unchanged. Its decay kinetics are significantly affected, though; the excimer lifetime is greatly enhanced by the reduction in temperature (compare intensity in the 2.1-2.4 eV range at 295 K and 100 K), consistent again with a suppression of non-radiative decay channels. It is striking that there is no corresponding change in the SGE (dimer) emission band. The growth and decay kinetics of the peak at 1.95 eV overlay perfectly over the full temperature range, demonstrating that there is no change in the formation mechanism (energy transfer), nature (i.e. extent of delocalisation) or radiative vs. non-radiative decay rates of this species. These observations are most consistent with a J-aggregated dimer which has very high PL quantum efficiency.

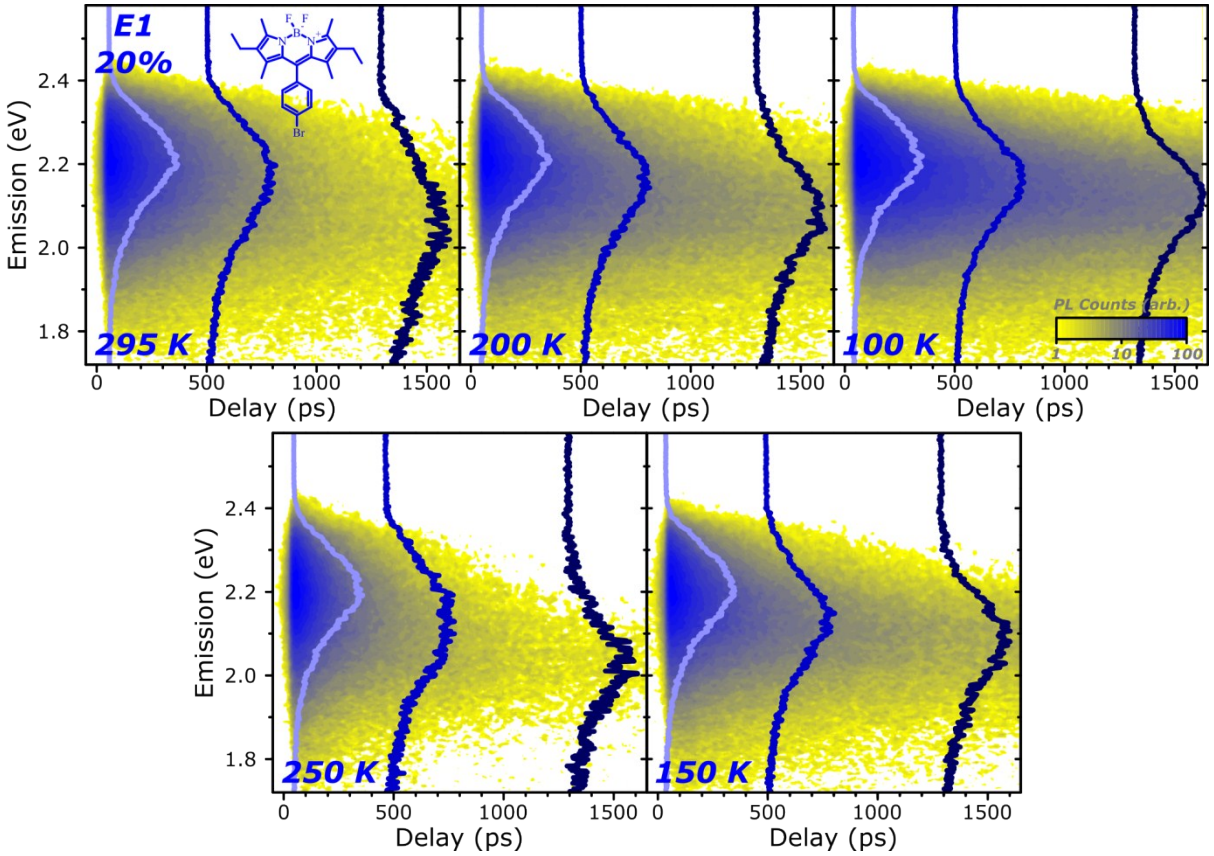

Figure S14. Fast PL dynamics of concentrated E1 films over the temperature range 295 – 100 K. At all temperatures the dynamics are consistent with two emissive species. The position of the initial monomeric emission is temperature-invariant, while the longest-lived signal shifts with temperature as the excimer identified from steady-state measurements. Spectral cuts (lines) taken at 50 ps (light blue), 500 ps (blue) and 1500 ps (dark blue) highlight the evolution of spectral shape following photoexcitation. The same logarithmic intensity scale is used for all plots, both to emphasize the contribution of weak, long-lived species and to reveal the increasing weight of excimer emission as the temperature is reduced.

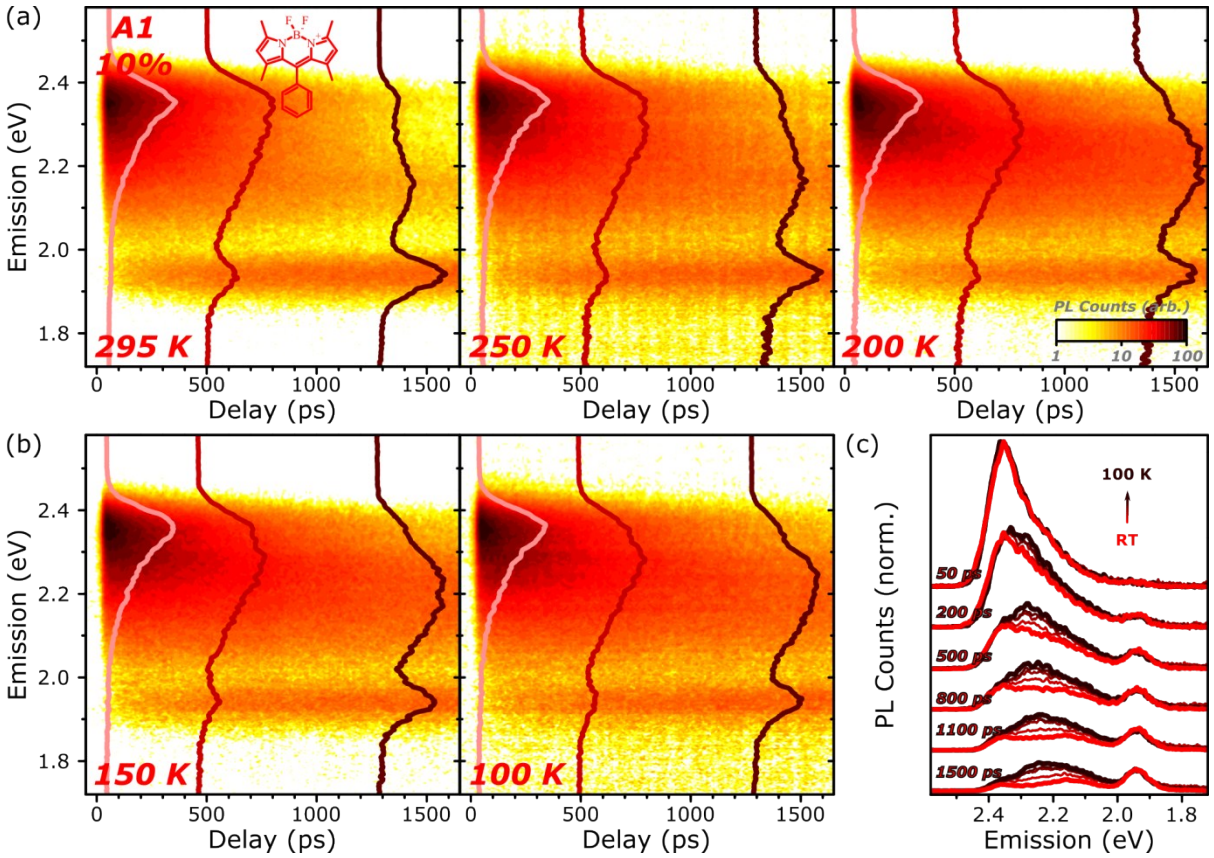

Figure S15. Fast PL dynamics of concentrated A1 films over the temperature ranges (a) 295 – 200 K and (b) 150 – 100 K. At all temperatures the dynamics are consistent with thee emissive species. The position of the initial monomeric emission is temperature-invariant, as are the SGE peaks (~1.95 eV) observed on long timescales. Similarly, the kinetic of SGE growth is completely invariant over the temperature range. Consistent with the steady-state measurements, the excimer species populated on intermediate timescales increases in relative intensity and shifts to higher energy upon cooling (emission ~2.2-2.3 eV). Spectral cuts (lines) taken at 50 ps (pink), 500 ps (red) and 1500 ps (dark red) highlight the evolution of spectral shape following photoexcitation. The same logarithmic intensity scale is used for all plots. (c) Spectral cuts across full decay range for each temperature from 295 K (red) to 100 K (dark red). Data for each temperature is separately normalised by the maximum intensity at 50 ps. The perfect overlap of initial spectra, emission band edge and SGE at 1.95 eV demonstrate that the initial state and SGE aggregate component are relatively unaffected by cooling. The differences between traces are due primarily to increasing weight of the shifting excimer band.

3.5 Long-Delay PL Dynamics

For delays beyond the temporal range of the streak camera, we performed TCSPC measurements on dilute films of E1 (0.1 %) and concentrated films of E1 (20%) and A1 (10%). Excitation was at 387 nm, and detection was scanned in 10 nm steps from 500 (2.48 eV) to 750 nm (1.72 eV) with equal acquisition time at each wavelength. This method enables reconstruction of the spectral shape on time delays out to 100 ns.

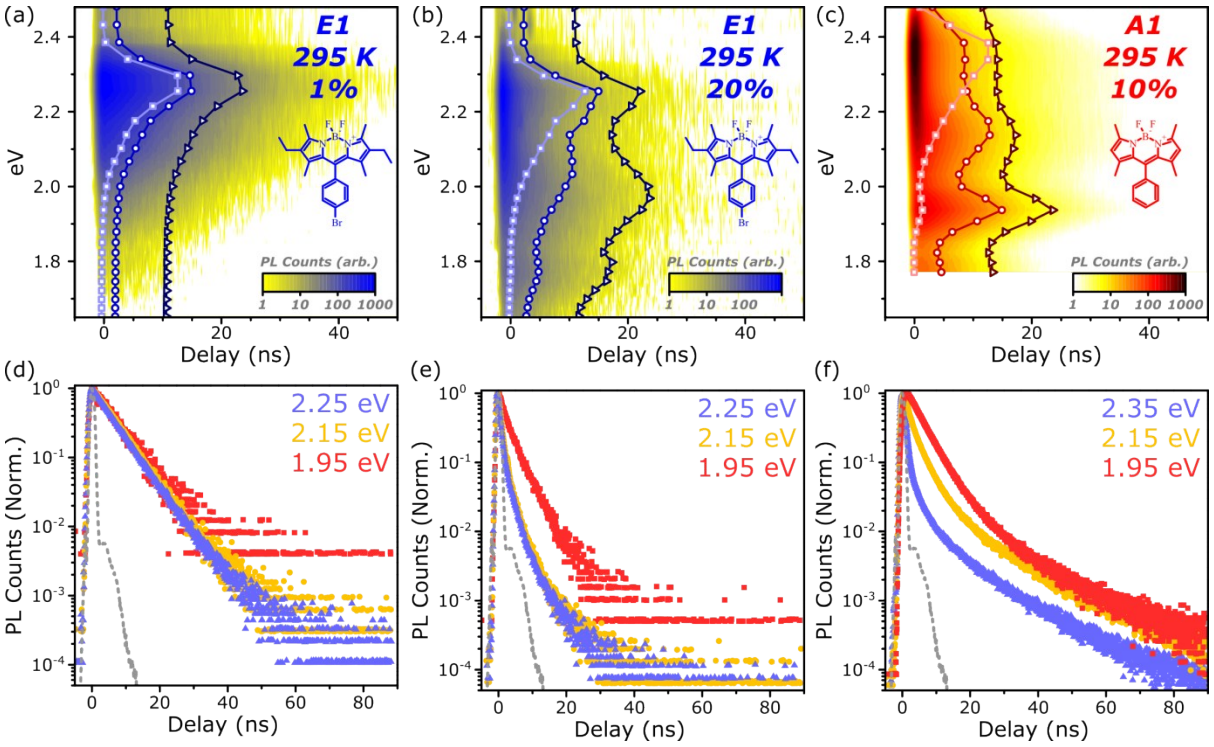

Figure S16. TCSPC maps of (a) dilute E1, (b) concentrated E1 and (c) concentrated A1. Spectral features agree with the species identified in streak-camera measurements. Note that the 1-2 ns instrument response conceals the fast dynamics measured with the streak camera and underestimates the degree of initial monomer decay. Normalized spectral slices at the peak of IRF (light blue/pink), 2.5 ns (blue/red) and 10 ns (dark blue/dark red) reveal evolution of spectral shape. Intensity scale is logarithmic to highlight contributions from weak long-lived states. Selected normalized decay kinetics in (d) dilute E1 reveal uniform monomer decay with a lifetime of 6.4 ns. The decays in (e) concentrated E1 are complex and non-exponential but can be approximately described with biexponentials with time constants 1 ns and 3.9 ns. Likewise in (f) concentrated A1, the final decay is distinctly non-exponential. The dominant lifetime of the SGE aggregate peak (1.95 eV) is 4.8 ns, though longer components are also present. Similar dynamics are observed in the LEMS region (2.15 eV), but on longer timescales this species appears to exhibit slightly longer lifetime (> 5 ns).

4. Transient Absorption

We performed transient absorption measurements on high-concentration (10%) films of A1 in vacuum to aid identification of the emissive state found in streak-camera measurements. The sample was held in vacuum and excited at 400 nm with a pump power of 800 µW. Because of the very weak signal strength of the long-lived states, it was not possible to obtain reasonable signal to noise at lower pump intensities. Data could not be obtained on low-concentration (1%) films due to the extremely low absorption cross-section. Due to the very low excited-state absorption cross-section of BODIPYs, the dominant signatures in Fig. S17 in all states are ground-state bleach and stimulated emission (ΔmOD<0). The initial monomer signature (blue, ~2.4 eV, compared to monomer from streak camera in red dashed) decays on similar timescales to the monomer lifetime observed in streak-camera measurements, giving rise to sharply structured negative bands <2.3 eV (light orange). These features exhibit a clear rise and thus are not significantly populated with the excitation pulse. The positions of these peaks align well with the peaks of extracted SGE (yellow dashed), and the fitted J-coupled dimer PL (pink dashed) and corresponding PL excitation (grey dashed). They can thus be assigned to stimulated emission from the longest-lived states, with a possible contribution as well from ground-state bleaching of the aggregate bands. Comparison of the spectra in Fig. S17c shows that the peak at ~2.2 eV very closely aligns with the LEMS shoulder of the SGE spectrum (yellow). It is thus likely that the band observed in this region contains contributions from both stimulated emission and bleaching of the J-coupled dimer absorption (grey). The very small signal level (~0.02, versus initial peak signal of 0.4 in the monomer region) is consistent with relatively small population in these states and agrees with the small SGE/Excimer branching ration obtained below.As in streak-camera measurements, the bands corresponding to LEMS (~2.2 eV) and J-coupled dimer (>2.0 eV) exhibit correlation in their rise dynamics, as befits their parallel population from the same parent (monomer) state. The mechanical delay stage was not long enough to establish whether their decay dynamics also agree.

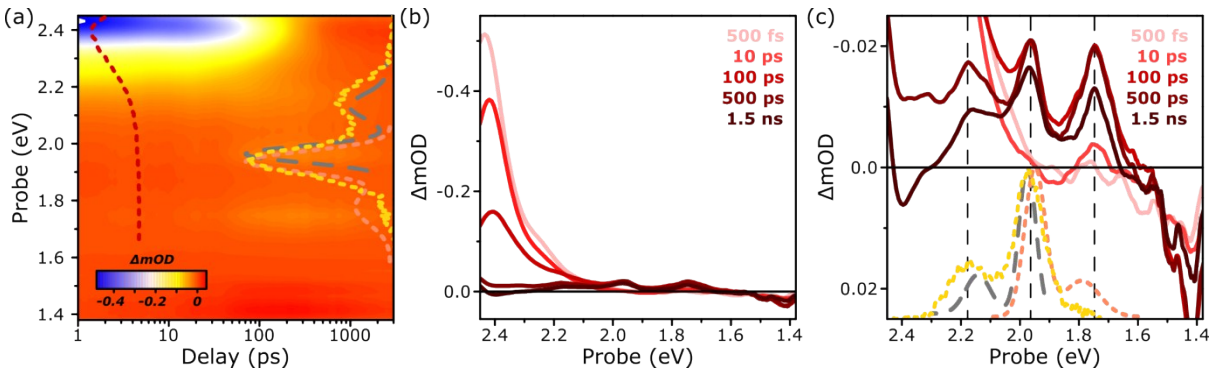

Figure S17. Transient absorption of concentrated A1 films. (a) False-color transient absorption map showing full evolution of excited-state signatures. Overlaid dashed spectra are taken from PL measurements for comparison to initial monomer (blue) and delayed SGE-type (light orange, from ~80 ps) transient absorption signatures: red – monomer emission, yellow – SGE spectrum, pink – fitted J-coupled dimer emission, grey – fitted J-coupled dimer PL excitation. (b) Selected timeslices of the data in (a), showing the rapid decay of the very large initial monomer signal and weak excited-state absorption. (c) Higher magnification of the same data, revealing growth of structured vibronic bands <2.3 eV on long timescales. Reference spectra (dashed) are same as in panel (a). Vertical dashed lines are a guide to the eye.

5. Radiative Rates and Branching Ratios

Using the extracted spectra in main-text Fig. 6, we can approximate the relative contribution of each species to the steady-state emission, population branching ratios and quantum efficiencies. The best fit of area-normalised species spectra gives the fraction of PL (F_{xxx}) arising from each species. The PL quantum yield (PLQY) was determined at room temperature. The low-temperature value was obtained based on the increase in PL intensity under cooling. Intrinsic monomer radiative rates were determined from the dilute (i.e. monomer-only) film data in Fig. S3c,d and the lifetime determined from TCSPC. The following parameters were used for this analysis:

	E1, 20%		**A1, 10%**	
	295 K	**100 K**	**295 K**	**100K**
PLQY *(dilute film)*	0.03 (*0.53*)	0.12 (*0.74*)	0.15 (*0.53*)	0.35 (*0.795*)
F_{Mon}	0.74	0.17	0.14	0.07
F_{Exc}	0.26	0.83	0.06	0.62
F_{Sge}	--	--	0.80	0.31

E1

In high-concentration E1 films, the excimer accounts for 26% of total emission, rising to 83% at 100 K. We consider three possible pathways for decay of the initial monomer excited state: radiative decay, non-radiative decay and excimer formation. The first two of these are intrinsic to the molecule and can be determined from dilute films in which no excimers are formed. From the rapid quenching of the monomer emission in 20% films, we can then extract that ~96% of photoexcitations form excimers. The PL quantum efficiency of the excimer varies from 0.01 at 295 K to 0.10 at 100 K, implying a radiative lifetime of ~500 ns.

From the PL lifetime in low-concentration films of 6 ns at 295 K (a typical value for monomeric BODIPY dyes), we obtain

$$k_{radMon} = \frac{PLQY}{\tau_{TotRT}} = (11.4\ ns)^{-1}$$

$$k_{nradMonRT} = \frac{(1 - PLQY)}{\tau_{TotRT}} = (12.8\ ns)^{-1}$$

where the subscript RT refers to 295 K, and we have assumed the monomer radiative rate is temperature-independent.

In concentrated films, we assume the monomer radiative and non-radiative decay rates are the same as in dilute, and the only other contribution to the monomer lifetime is excimer formation. We can then extract the rates of excimer formation k_{Exc}:

$$PLQY_{MonConcRT} = PLQY_{ConcRT} * F_{MonRT} = 0.022 = \frac{k_{radMon}}{k_{radMon} + k_{nradMonRT} + k_{ExcRT}} =$$

$$\rightarrow k_{ExcRT} = (263\ ps)^{-1}$$

This result is consistent with the measured monomer lifetime of 250 ps, confirming our assumptions are appropriate. This rate of excimer formation implies that >90% of excitations form excimers (φ_{Exc}), resulting in the following E1 excimer PLQYs:

$$\varphi_{ExcRT} = \frac{k_{ExcRT}}{k_{radMon} + k_{nradMonRT} + k_{ExcRT}} = 0.96$$

$$PLQY_{ExcRT} = \frac{PLQY_{ConcRT} * F_{ExcRT}}{\varphi_{ExcRT}} = \frac{0.03 * 0.26}{0.96} = 0.008$$

We note here that F_{Exc} refers explicitly to the fraction of emitted photons from the excimer state, whereas φ_{Exc} is the fraction of the total population that forms an excimer. The same analysis can be performed for the low-temperature results.

100 K:

$$k_{nradMonLT} = (32.3\ ns)^{-1}$$

$$PLQY_{MonConcLT} = PLQY_{ConcLT} * F_{MonLT} = 0.02 = \frac{k_{radMon}}{k_{radMon} + k_{nradMonLT} + k_{ExcLT}} =$$

$$\rightarrow k_{ExcLT} = (239\ ps)^{-1}$$

$$PLQY_{ExcLT} = \frac{PLQY_{ConcLT} * F_{ExcLT}}{\varphi_{ExcLT}} = \frac{0.12 * 0.83}{0.97} = 0.10$$

A1

Applying the same procedures to A1 10% films, we find that the excimer contributes only 6% to the total PL at room temperature, while the SGE contributes 80%. At 100 K the excimer weight increases to 62%, with 31% arising from SGE. In order to determine the branching ratios from the observed dynamics, we have used the facts that the absolute yield of SGE PL is temperature independent. Based on our energy-transfer mechanism of excimer/SGE formation and the ~constant formation kinetics at all temperatures, we know that the fraction of SGE states formed should not substantially change upon cooling. The insensitivity of SGE emission to cooling thus implies a negligible rate of non-radiative decay, i.e. near-unity quantum yield.

We apply a similar analysis to films of A1 as for E1. From the fraction of monomer emission detected in high concentration films and the measured decay lifetime of 190 ps:

$$k_{radMon} = \frac{PLQY_{MonConcRT}}{\tau_{MonConc}} = \frac{PLQY_{ConcRT} * F_{MonRT}}{\tau_{MonConc}} = \frac{0.15 * 0.14}{(190\ ps)^{-1}} = (9\ ns)^{-1}$$

$$k_{nradMonRT} = \frac{1 - PLQY_{DilRT}}{PLQY_{DilRT}} k_{radMon} = \frac{1 - 0.53}{0.53} (9\ ns)^{-1} = (10\ ns)^{-1}$$

$$k_{nradMonLT} = \frac{1 - PLQY_{DilLT}}{PLQY_{DilLT}} k_{radMon} = \frac{1 - 0.795}{0.795} (9\ ns)^{-1} = (35\ ns)^{-1}$$

where we have assumed the radiative decay rate is independent of temperature and film concentration. The total rate of formation of intermolecular species can then be extracted:

295 K:

$$PLQY_{MonConcRT} = PLQY_{ConcRT} * F_{MonRT} = 0.021 = \frac{k_{radMon}}{k_{radMon} + k_{nradMonRT} + k_{ExcRT} +}$$

$$\rightarrow$$

$$k_{ExcRT} + k_{SgeRT} = (197\ ps)^{-1}$$

$$\varphi_{ExcRT} + \varphi_{SgeRT} = \frac{k_{ExcRT} + k_{SgeRT}}{k_{radMon} + k_{nradMonRT} + k_{ExcRT} + k_{SgeRT}} = \frac{(197\ ps)^{-1}}{(9\ ns)^{-1} + (10\ ns)^{-1} + (197\ ps)^{-1}} = 0.96$$

100 K:

$$PLQY_{MonConcLT} = PLQY_{ConcLT} * F_{MonLT} = 0.021 = \frac{k_{radMon}}{k_{radMon} + k_{nradMonLT} + k_{ExcLT} +}$$

$$\rightarrow$$

$$k_{ExcLT} + k_{SgeLT} = (228\ ps)^{-1}$$

$$\varphi_{ExcLT} + \varphi_{SgeLT} = \frac{k_{ExcLT} + k_{SgeLT}}{k_{radMon} + k_{nradMonLT} + k_{ExcLT} + k_{SgeLT}} = \frac{(228\ ps)^{-1}}{(9\ ns)^{-1} + (34\ ns)^{-1} + (228\ ps)^{-1}} = 0.97$$

We assume based on the temperature invariance of the SGE formation kinetics (which can be directly observed) that the formation rates of SGE and excimer are temperature independent: otherwise we would measure a distinct change in the monomer decay and SGE growth kinetics. This is reasonable, as the spatial density of SGE vs excimer-capable sites in the film should not be strongly affected by cooling. Given that the yield of SGE+excimer is virtually identical at room and low temperature (0.96 vs 0.97), this means that $\varphi_{ExcRT} \sim \varphi_{ExcLT}$ and $\varphi_{SgeRT} \sim \varphi_{SgeLT}$. Moreover, from the

temperature independence of the steady-state SGE emission we deduce that $PLQY_{SgeRT} \sim PLQY_{SgeLT}$. This leads to the series of equations:

$$PL_{SgeRT} = F_{Sge} * PL_{Tot} = 0.80 * 0.15 = 0.12$$

$$= PLQY_{Sge} * \frac{k_{SgeRT}}{(9\ ns)^{-1} + (10\ ns)^{-1} + (197\ ps)^{-1}}$$

$$PL_{ExcRT} = F_{Exc} * PL_{Tot} = 0.06 * 0.15 = 0.009$$

$$= PLQY_{ExcRT} * \frac{k_{ExcRT}}{(9\ ns)^{-1} + (10\ ns)^{-1} + (197\ ps)^{-1}}$$

$$PL_{SgeLT} = F_{SgeLT} * PL_{Tot} = 0.31 * 0.35 = 0.11$$

$$= PLQY_{Sge} * \frac{k_{SgeLT}}{(9\ ns)^{-1} + (34\ ns)^{-1} + (228\ ps)^{-1}}$$

$$PL_{ExcLT} = F_{ExcLT} * PL_{Tot} = 0.62 * 0.35 = 0.22$$

$$= PLQY_{ExcLT} * \frac{k_{ExcLT}}{(9\ ns)^{-1} + (34\ ns)^{-1} + (228\ ps)^{-1}}$$

Varying the PLQY of the SGE state, we can fully determine the other parameters as follows:

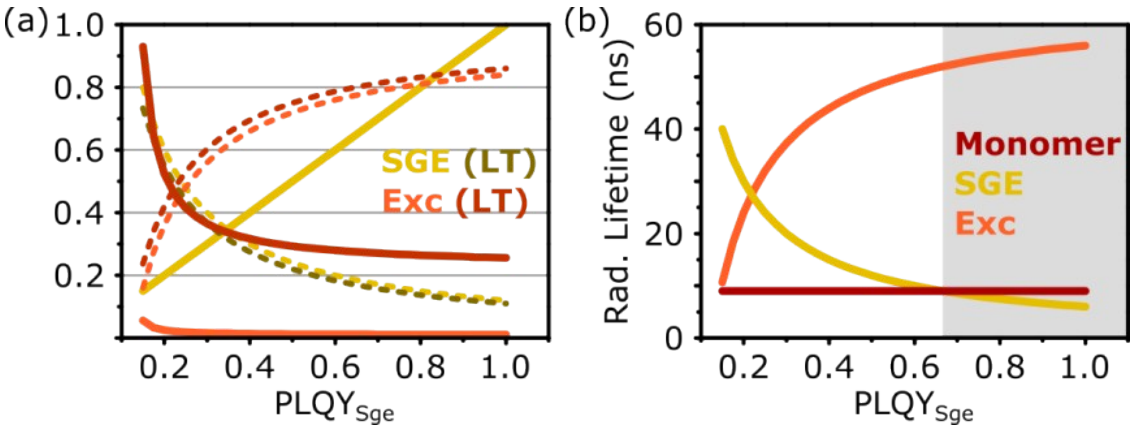

Figure S18. Population branching and radiative rates. (a) PLQY (solid) and population fraction φ_{xxx} (dashed) of SGE and excimer states at 295 K (light) and 100 K (dark), as a function of the SGE PLQY. (b) Corresponding radiative lifetimes of SGE and excimer, assuming that the radiative rate is temperature-independent in both states. In the region highlighted grey, the SGE radiative lifetime is shorter than the monomer lifetime, consistent with J-type coupling.

Only at the upper limits of $PLQY_{SGE}$ are the results consistent with our other observations: SGE lineshape indicative of J-type excitonic coupling, approximately equal excimer-SGE branching ratio at low and high temperature, and very low excimer PLQY at 295 K with correspondingly long radiative rate. We thus extract that $PLQY_{SGE}$~1, $PLQY_{Exc}$~0.01 (0.26) at 295 K (100 K), φ_{Sge}~0.12 and φ_{Exc}~0.84.

6. References

1 G. Nöll, J. Daub, M. Lutz and K. Rurack, *J. Org. Chem.*, 2011, **76**, 4859–4873.

2 A. B. Nepomnyashchii, M. Bröring, J. Ahrens and A. J. Bard, *J. Am. Chem. Soc.*, 2011, **133**, 8633–8645.

3 H. Imahori, H. Norieda, H. Yamada, Y. Nishimura, I. Yamazaki, Y. Sakata and S. Fukuzumi, *J. Am. Chem. Soc.*, 2001, **123**, 100–110.

4 D. Aydın Tekdaş, G. Viswanathan, S. Zehra Topal, C. Y. Looi, W. F. Wong, G. Min Yi Tan, Y. Zorlu, A. G. Gürek, H. B. Lee and F. Dumoulin, *Org. Biomol. Chem.*, 2016, **14**, 2665–2670.

5 H. Lu, Q. Wang, L. Gai, Z. Li, Y. Deng, X. Xiao, G. Lai and Z. Shen, *Chem. - A Eur. J.*, 2012, **18**, 7852–7861.

6 L. Gai, J. Mack, H. Lu, H. Yamada, D. Kuzuhara, G. Lai, Z. Li and Z. Shen, *Chem. - A Eur. J.*, 2014, **20**, 1091–1102.

7 Z. Yang, Y. He, J. Lee, N. Park, M. Suh, W.-S. Chae, J. Cao, X. Peng, H. Jung, C. Kang and J. S. Kim, *J. Am. Chem. Soc.*, 2013, **135**, 9181–9185.

8 N. Gupta, S. I. Reja, V. Bhalla, M. Gupta, G. Kaur and M. Kumar, *Chem. Commun.*, 2015, **51**, 10875–10878.

9 R. T. Grant, P. Michetti, A. J. Musser, P. Gregoire, T. Virgili, E. Vella, M. Cavazzini, K. Georgiou, F. Galeotti, C. Clark, J. Clark, C. Silva and D. G. Lidzey, *Adv. Opt. Mater.*, 2016, **4**, 1615–1623.